Usage of polarization for high-accuracy micro-metrology sensors

M. Totzeck, H. Jacobsen, H. J. Tiziani
Institut für Technische Optik, Universität Stuttgart, D-70569 Stuttgart, Germany

ABSTRACT

The general idea of the presented investigations is to use the polarization of the electromagnetic field in high-resolution optical microscopy to get information about sub-wavelength details of topographical structures. The main application is the localization of vertical edges. For structures in non-magnetic materials, polarization effects are caused by the different boundary conditions for the tangential and normal electric field components. Using rigorous numerical simulations we show that two physical-optics model describe the polarization dependent images of vertical edges and sub-wavelength structures: a boundary diffraction wave originating from the tip of the edge and waveguiding effects, respectively. We report on two experimental approaches for polarization usage: a) comparison of interference microscopy images for s- and p-polarization, and b) polarization interferometry. The former is capable of „synthetical microscopy". Measurements of well defined structures (calibrated with a scanning force microscope) are compared with rigorous numerical simulations.

Keywords: Metrology, polarization microscopy, CD measurements, boundary conditions, numerical simulation

1. INTRODUCTION

Optical inspection of surfaces has the well known advantages of a minimum interaction with the object and high measurement rates. All this at comparatively low technical expense. The not less well known main problem is the Rayleigh resolution limit, i.e. limitation of the resolution to the half wavelength. This is crucial for the microstructures considered in ths contribution (Fig. 1). However, the reproducibility of optical measurements is much better than the resolution: in principle it is possible to localize the position of an isolated edge according to threshold- or extreme-value criteria[1] with <1nm precision. Although a precision of 3 nm is state of the art, deviations of up to 100 nm to the true edge position are observed.[2] The reason for the decreased accuracy is the assumption of a reflection (or transmission) according to geometrical optics neglecting physical-optics effects. The electromagnetic boundary conditions provide a polarization dependent edge scattering resulting in polarization dependent threshold values. If edges are closely neighbored, multiple scattering occurs, resulting in an even increased polarization dependence. These polarization dependence must be known and understood in order to correct microscopical measurements, i.e. to calibrate the sensor. To this end, physical-optics models are very useful.

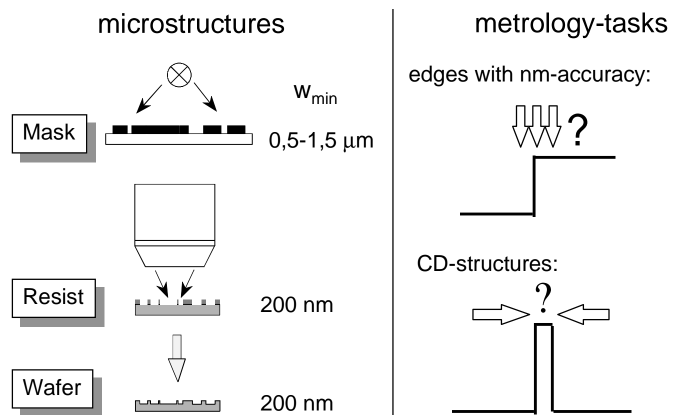

Fig. 1: Objects and tasks of optical micrometrology

Microstructures of main interest are photomasks, resist on silicon and etched wafers with a critical dimension of now <200 nm (Fig. 1a). For the present investigation, we restrict ourselves to pure topographical isolated edges or line structures down to sub-wavelength width (Fig. 1b).

From a physical optics point of view, usage of the polarization in micro-metrology means to perform measurements of structure dimensions that take two different boundary conditions as a basis. The advantages are obvious. For example:

Correspondence: MT: totzeck@ito.uni-stuttgart.de ,HJ: jacobsen@ito311.ito.uni-stuttgart.de HT: tiziani@ito311.ito.uni-stuttgart.de, phone: ++49.711.685.6074, fax: ++49.711.685.6586, www http://uni-stuttgart.de/UNIuser/ito/

a) increased accuracy of threshold-value measurements, for instance by finding an optimum polarization

b) simultaneous imaging and detection of regions where the boundary conditions differ. The signal strength depends on the amount of the difference which itself depends on edge-material and –angle. This enables a discrimination of a damaged or soiled edge from an edge at the wrong position.

c) structure characterization where no spatial information is available, as for sub-wavelength gratings.[3]

In a restricted sense, polarization usage means the generation of contrast from the polarization difference, i.e. from the fact that the x-polarized image $E_x(x,y)$ does not equal the y-polarized image $E_y(x,y)$.[18] This could be done, for instance, by the crossed polarizer configuration[4,5] (image = $|E_x^2 + E_y^2|$) or polarization interferometry[6] (image = $E_x E_y^*$). However, several more contrast-mechanisms (i.e. functions of E_x and E_y) are possible.[19] Which should be applied for a given structure and illumination and what systematical errors should we expect? In our contribution we try to present a method to answer these questions.

The organization of the paper is as follows: In the next section we explain the measurement of complex fields with interference microscopy. Then we present measured and computed polarization effects in section 3 and discuss their physical optics origin in terms of boundary diffraction waves and waveguiding effects in section 4. An interferometrical method to use polarization effects for enhanced edge detection are presented in section 5.

2. COMPLEX FIELD MEASUREMENT WITH INTERFERENCE MICROSCOPY

For a systematical investigation of the influence of polarization on the image of line-structures we employed a Linnik-type interference microscope that is equipped with a linear polarizer in the illuminating section. We will show that it enables a measurement of the diagonal elements of the Jones-matrix of the object. This provides a direct measure for the polarization effect due to the structure. Furthermore, we can perform ”synthetical microscopy”, which means that we can take the complex field as basis to perform typical microscopic operations, like focusing, polarization contrast, or dark-field contrast, subsequently in the computer.

2.1 Interference microscopy set-up

The interference microscope is based on a modified LEICA-Orthoplan 100. The optical system is sketched in Fig. 2. A mercury high-pressure lamp (HBO50) with subsequent interference filter (λ=549nm, $\Delta\lambda$=20nm) polarizer and adjustable aperture stop provides an approximately monochromatic, linearly polarized, partially coherent illumination with adjustable coherence parameter (ratio of illumination NA and imaging NA) between 0.2 and 0.95. For the present investigations, a coherence parameter of 0.2 was used.

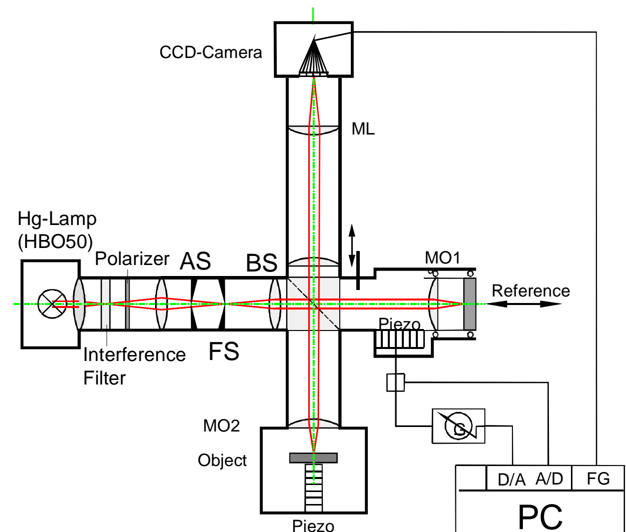

Fig. 2: Linnik-type interference microscope (MO1, MO2: paired microscope lenses, ML: magnifying lens system, AS: aperture-stop, FS: field-stop)

The images of the investigated structure and a plane reference mirror, provided by two paired microscope lenses (100x, NA=0.9), are superposed by a beamsplitter onto a CCD-camera chip with 8.2 x 9.4 µm-pixel pitch (Hitachi KP160). A second magnifying lens-system in front of the CCD-camera yields an additional 4x-magnification with the consequence that the system operates in the regime of empty magnification with an object distance of 21 nm between adjacent camera-pixels. The image is sampled with 10 bit resolution using a MV1000 frame-grabber. With proper adjustment, high-contrast, straight interference fringes can be observed even for white light illumination.

The noise is reduced by two means: 1) 10 frames are averaged for each interferogram. 2) Because of the high magnification the interferograms may be low-pass filtered considerably without affecting the lateral resolution. With λ=549nm, M=400 and 9µm pixel-size, NA_{Ill}=0.25, NA_{Img}=0.9, the cut-off frequency of $1.1/\lambda$ in the object plane is equivalent to a cut-off frequency of 24 $pixel^{-1}$ in the image plane. Therefore, each interferogram is low-pass filtered using a Gaussian filter with a standard deviation of 2 pixel.

2.2 Interferogram-evaluation for vector fields

The interferogram on the CCD chip stems from the vector field $\mathbf{E_O}$ due to the object and a phase shifted reference field $\mathbf{E_R}$ according to (to simplify the notation, the spatial dependence is not written)

$$I_{\Delta\varphi} = \left|\mathbf{E_O} + \mathbf{E_R}\exp(i\Delta\varphi)\right|^2 \tag{1}$$

that becomes in the usual form

$$\mathrm{I}_{\Delta\varphi} = \mathrm{I_g}\left(1 + \gamma\cos(\phi + \Delta\varphi)\right) \tag{2}$$

with phase ϕ, intensity I_g, and contrast γ

$$\begin{aligned} I_g &= \left|\mathbf{E_O}\right|^2 + \left|\mathbf{E_R}\right|^2 \\ \gamma &= \frac{2\left|\mathbf{E_O}\cdot\mathbf{E_R}\right|}{I_g} \\ \phi &= \arg\left(\mathbf{E_O}\cdot\mathbf{E_R^*}\right) \end{aligned} \tag{3}$$

The measurement is performed according to the eight-step method of phase-shift interferometry[7]: 8 images I_j (j=1-8) are captured where the j'th component is phase-shifted by $\beta_j = j\pi/2$. Phase ϕ, intensity $I_0 = I_g$, and contrast γ are obtained by

$$\tan\phi(x,y) = \frac{Z}{N} \tag{4}$$

and

$$\gamma(x,y) = \frac{\sqrt{Z^2 + N^2}}{32 I_0} \tag{5}$$

with

$$\begin{aligned} Z &= 5I_2 - 15I_4 + 11I_6 - I_8 \\ N &= I_1 - 11I_3 + 15I_5 - 5I_7 \\ I_0 &= \tfrac{1}{8}\sum_{j=1}^{8} I_j \end{aligned} \tag{6}$$

The phase-shift is performed either by moving the reference lens and mirror simultaneously (the reference mirror is always in focus) with a piezo or by defocusing the object using a piezo-driven table (Physik-Instrumente). The z-position of the piezo-driven table is actively stabilized using capacitive sensors with sub-nm resolution. We used for the present investigations the phase shift of the reference because for an object-defocus the well known aperture factor of interference microscopy[8] has to taken into account.

According to (3), the scalar, complex quantity $\mathbf{E_O}\mathbf{E_R}^*$ is obtained from

$$\mathbf{E_0}\cdot\mathbf{E_R^*} = 0.5\gamma \mathrm{I_g}\exp(\mathrm{i}\phi) \tag{7}$$

If we ensure normally incident, plane, linearly polarized reference wave along the x- and y-direction, i.e.

$$\mathbf{E_x^R} = \begin{pmatrix}1\\0\end{pmatrix} \quad \text{and} \quad \mathbf{E_y^R} = \begin{pmatrix}0\\1\end{pmatrix} \tag{8}$$

we get from Eq. (4) the complex field components $\mathbf{E_x^O}$ and $\mathbf{E_y^O}$.

Demanding a linearly polarized reference wave implies an optics without depolarizing elements. However, we used an interference microscope without particular strain-free lenses and without a non-depolarizing beam-splitter. Experiments have shown, that the main source for polarization-anisotropy in the set-up is the beam-splitter. Due to its construction a beam-

splitter has two orthogonal eigenpolarizations along which no depolarization occurs. We have chosen these directions as the x- and y-axis of the global coordinate system.

For each structure, two measurements are performed, with an incident x-polarized and an incident y-polarized wave, respectively.

The intensity $I=|E|^2$ of the object wave can be measured separately by inserting a stop into the reference arm. Combined with Equ. (3) we may also obtain the complex object wave from

$$E = I^{1/2} \exp(\phi(x, y)) \tag{9}$$

This straight forward expression has the advantage of being independent from intensity-variations of the reference. But it may lead to inconsistencies as will be shown below.

Eq. (7) and (9) are equivalent if no depolarization occurs at the structure. This is the case, for instance, for a line structure and an incident wave polarized parallel or perpendicular to its edges. In our coordinate system, the configuration has a diagonal Jones-matrix if the edges are oriented along the x- and y-axis

$$\mathbf{E_0} = \begin{pmatrix} J_{xx} & 0 \\ 0 & J_{yy} \end{pmatrix} \mathbf{E_i} \quad \text{with} \quad \mathbf{E_i} = \begin{pmatrix} 1 \\ 0 \end{pmatrix} \text{or } \mathbf{E_i} = \begin{pmatrix} 0 \\ 1 \end{pmatrix} \tag{10}$$

For a depolarizing structure, i.e. a configuration with a Jones-matrix with non-diagonal elements, we get

$$\mathbf{E_0} = \begin{pmatrix} J_{xx} & J_{xy} \\ J_{yx} & J_{yy} \end{pmatrix} \mathbf{E_i} = \begin{pmatrix} J_{xx} \\ J_{yx} \end{pmatrix} E_x^i + \begin{pmatrix} J_{xy} \\ J_{yy} \end{pmatrix} E_y^i \tag{11}$$

Assuming a perfectly reflected reference wave we set $\mathbf{E_R}=\mathbf{E_i}^*$ and get

$$\mathbf{E_0} \cdot \mathbf{E_R} = J_{xx}\left|E_x^i\right|^2 + J_{yy}\left|E_y^i\right|^2 + J_{xy}E_y^i E_x^{i*} + J_{yx}E_x^i E_y^{i*} \tag{12}$$

which becomes J_{xx} for a x-polarized and J_{yy} for a y-polarized incident wave, i.e. we measure separately the diagonal elements of the Jones-matrix even if non-diagonal elements are present. But in. Eq. (9) the intensity obtained with shut reference arm, includes the non-diagonal-elements

$$I_O = \left(\left|J_{xx}\right|^2 + \left|J_{yx}\right|^2\right)\left|E_x^i\right|^2 + \left(\left|J_{yx}\right|^2 + \left|J_{yy}\right|^2\right)\left|E_y^i\right|^2 \tag{13}$$

While the phase ϕ according to Eqs. (3) and (4) does not.

2.3 Example for synthetical microscopy: a-posteriori focusing

Consider a trench of 121 nm depth and 710 nm width in a Silicon substrate. For a linearly polarized, perpendicularly incident plane wave of 549nm wavelength, the reflected, complex field is imaged according to section 2.1 and 2.2. The obtained amplitude and phase are shown in Fig. 3.

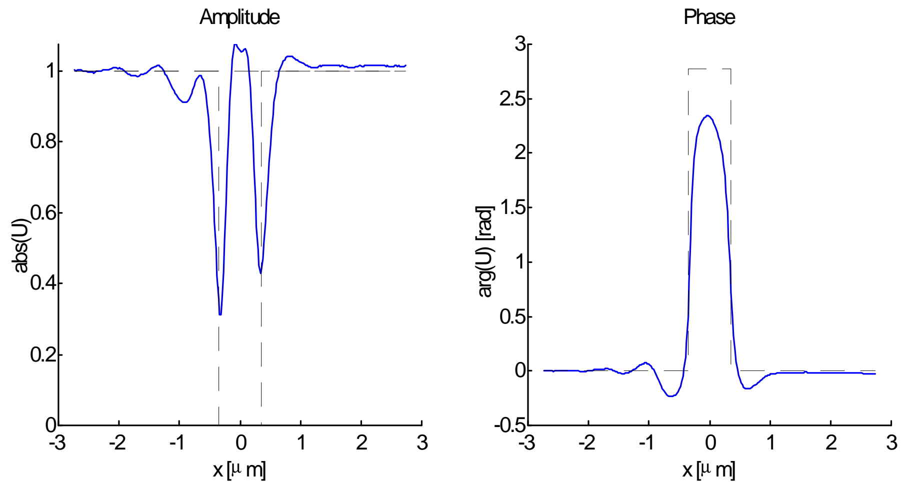

Fig. 3: Left: amplitude, right: phase measured at a Si trench of 710 nm width and 121nm depth in Si.

The incident wave is not perfectly coherent, because the

finite half-width of the applied interference filter ($\Delta\lambda$ = 20 nm) and the non-zero coherence parameter. With an illumination NA of 0.25, the coherence parameter becomes 0.28. Assuming a coherent field $U(x,y,z)$ we may compute a defocus of Δz from a focusposition $z=z_0$ according to

$$U(x,y,z_0+\Delta z)=F^{-1}\left\{F\left\{U(x,y,z_0\right\}\exp\left[i\left(k_0^2-k_x^2-k_y^2\right)^2\Delta z\right]\right\} \tag{14}$$

where F{ } denotes the Fouriertransform and F^{-1} { } its inverse. k_0 is the free space propagation constant and k_x and k_y are the spatial frequency components in x- and y-direction, respectively. Aberrations of the optical system could be included into Equ. (13), but this was not done here.

Fig. 4 shows a comparison of a computed intensity focus scan (left) and a measured one (right).

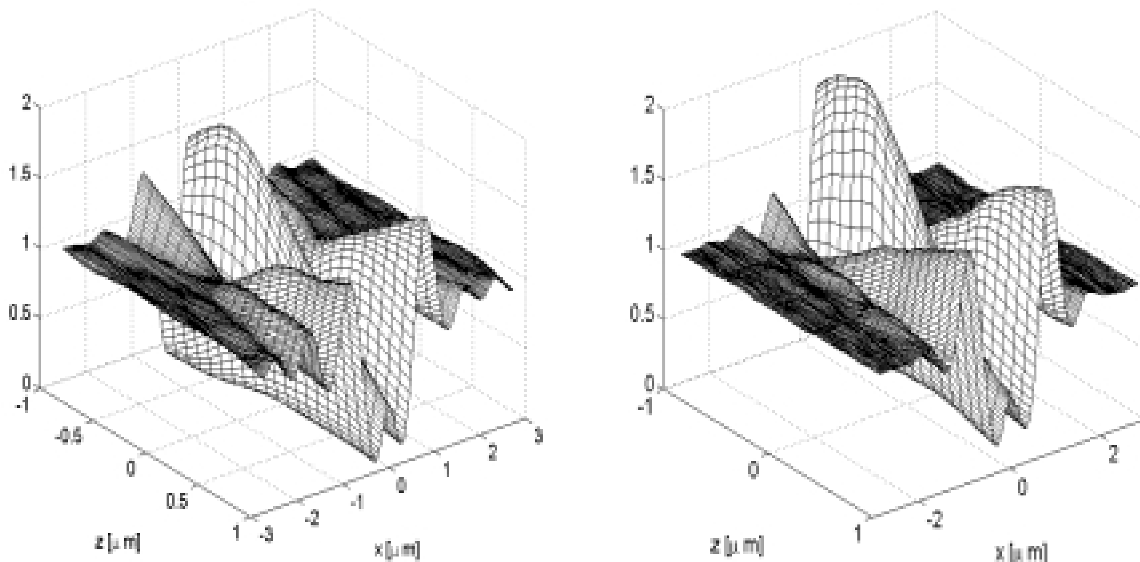

Fig. 4: Comparison of synthetic (left) and measured defocus (right) at a Si trench of 710 nm width and 121nm depth in Si

The agreement is satisfactorily. The main discrepancy is observed in the central peak for negative defocus (here: above the structure). Notice the higher diffraction lobes in the synthetic defocus. This stems from the fact that the mesurement is performed with a partially coherent wave field while the computed defocus according to Eq. (14) assumes a perfectly coherent wave field.

3. POLARIZATION EFFECTS IN COHERENT MICROSCOPY

Using the field measuring capability of interference microscopy and a rigorous numerical simulation of the imaging process we will give in this section an account of polarization effects observed in the images of topographical line structures. In particular we will investigate wide structures and small lines of sub-wavelength width. The structures are oriented parallel to the y-axis. They are etched into silicon that has an ellipsometrically determined refractive index of n=3.8+i*0.3 at λ=633nm. The refractive index of bulk Si is according to Ref. 9 is n=3.882+i*0.019 at λ=633nm, i.e. the real part agrees well but the imaginary part is significantly higher in our measurement. At our measurement-wavelength of 549nm, Ref. 9 gives a value of n=4.18+i*0.04 for the refractive index of Si. Having the increased imaginary part at HeNe wavelengths we assume that the imaginary part for our samples is also higher at λ=549nm. Therefore we used a refractive index of n=4.2+i*0.3 for a comparison with the interference microscopy measurements.

The focus position for the investigated small structures is adjusted visually so that the intensity above the structure shows two closely neighbored, sharp minima and a „coherent ringing“ that is at most close to the structure edges. This is not a strict but a sufficient focus criterion for the present investigation.

For a rigorous computation of the near-fields and coherent images of semiconductor structures, we developed a procedure based on the rigorous coupled wave theory (RCWA[10]) and Hopkins image formation theory using the effective source[11].

3.1 Wide trench

The first considered structure is a trench of 910 nm width and 121 nm depth. Both values are determined by scanning force microscopy. Fig. 5 shows amplitude and phase of the measured field components (circles) and the rigorous simulations (lines). For comparison the geometrical optics phase shift is included into the phase images.

Evidently, the modulation of amplitude and phase is stronger if the electric field vector is oriented perpendicular to the structure edges (TM-polarization) than in TE-polarization where it is oriented parallel to the edges. The edges are parallel to the y-axis. From a metrological point of view TM polarization seems to be better suited for edge localization of the present structure than TE-polarization. Despite this difference the agreement of the phase half-width and also of the amplitude minima with the actual structure edges is quite well.

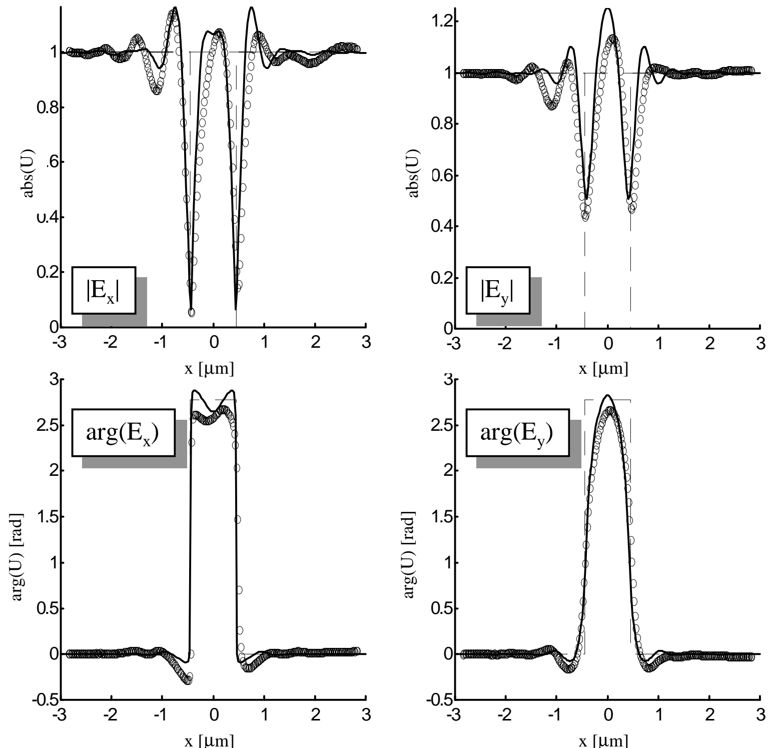

Fig. 5 Amplitude (top) and Phase (bottom (o: measurement, -: computation) of a Si trench of 910 nm width and 121nm depth in Si. left: TM-Pol., right: TE-Pol

Unfortunately, the conclusions from the above paragraph are not a general behavior: it depends on the structure depth as is demonstrated in Fig. 6, where a rigorous computation of the amplitude of edge images for steps of various heights (0-500 nm) is shown. The height is increasing from top to bottom.

The focus position is fixed to the top of the edge. The minimum is indicated by a solid line. It shows oscillations in accordance with the phase shift introduced by the step. However, the oscillations are more pronounced and more regularly in TM than in TE polarization. The difference becomes stronger with increasing illumination NA. Furthermore, the minimum is shifted away from the edge. Therefore, the minimum detection method for edge localization provides problems with increasing structure height.

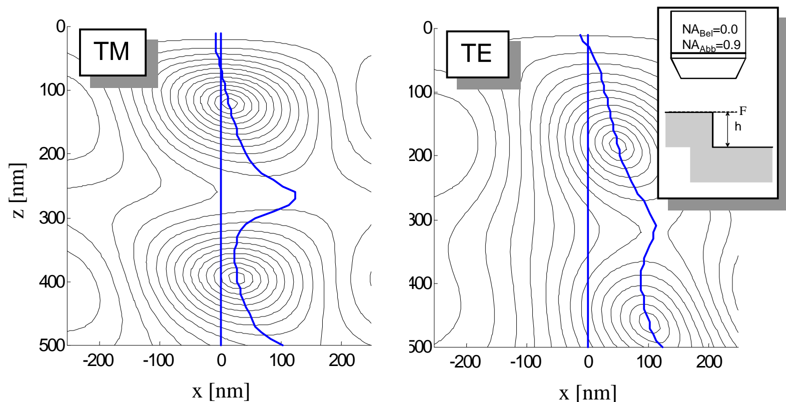

Fig. 6 Thickness-dependence of minimum-position at an Si-edge

3.2 Signal strength of sub-λ line

As is well known, the difference of TE and TM polarized images increases with decreasing line width. The effect for complex images is demonstrated in Fig. 7. The experimental parameters are identical to Fig. 5 but now the object is a trench of only 210 nm width. The observed amplitude modulation is distinctively stronger in TM than in TE polarization. I.e. the scattering cross section is higher in TM polarization. In TM polarization, two minima are still discernible with a distance of approximately 200nm, while they have already merged in TE polarization. An interesting phenomenon is observed in the phase image: The sign of the phase and therefore the apparent topography is opposite for both polarizations.

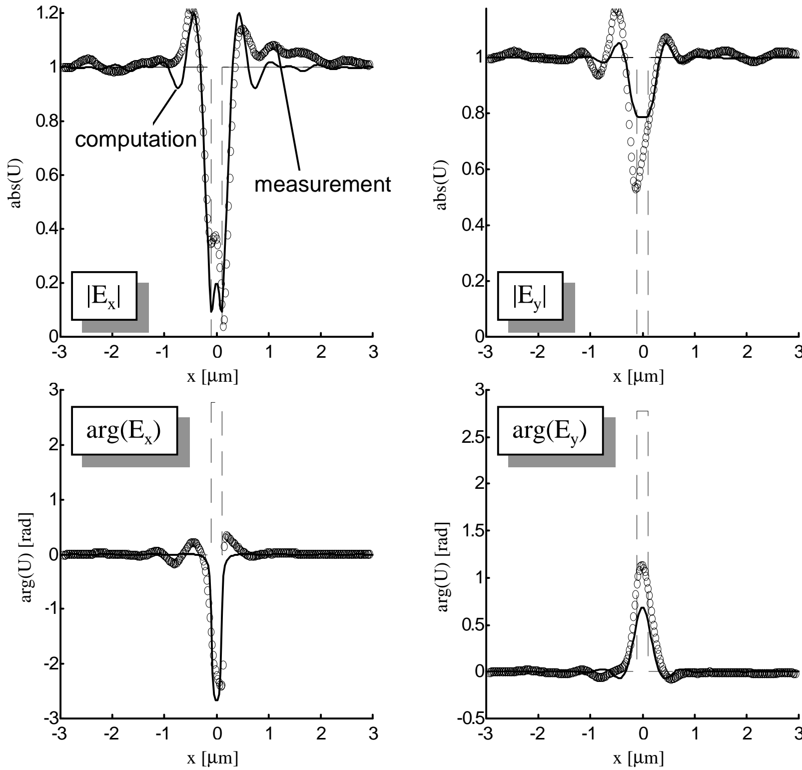

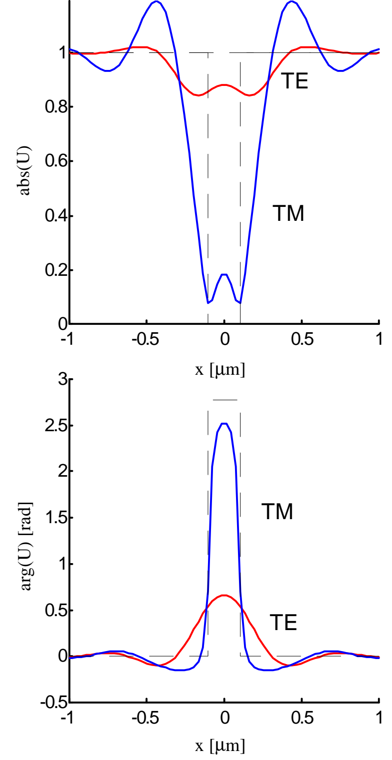

Fig. 7 Amplitude (top) and Phase (bottom) of a Si trench of 210 nm width and 121nm depth in Si. left: TM-Pol., right: TE-Pol

Fig. 8 Computed field of Fig. 7 with 120nm defocus.

The reason for the latter behavior is the close proximity of two phase-singularities[12] to the focus plane in TM-polarization. Phase-singularities are points in a wave-field where the intensity is zero with the consequence that the phase is not defined. Crossing the plane where the singularities have formed results in an approximately inverted phase-image. This is a consequence of the general property of phase singularities that crossing them yields a π-phaseshift. Here, a slight negative defocus crosses the singularity plane and removes the effect (Fig. 8).

Concluding this section we discuss what happens if we actually reverse the structure, i.e. if we image a bar of 210 nm width and 121 nm height. A comparison of both cases is shown in Fig. 9. Because the structure was not available, only computations are shown. The images have changed strongly: The general modulation is stronger and the amplitude images have become more alike. This is also true for the phase, although the sign is still reversed. Now, the half width of the phase-image as well as the minima in the amplitude image yield a comparatively large deviation from the actual edge position, i.e. they are less valid indicators for the true linewidth.

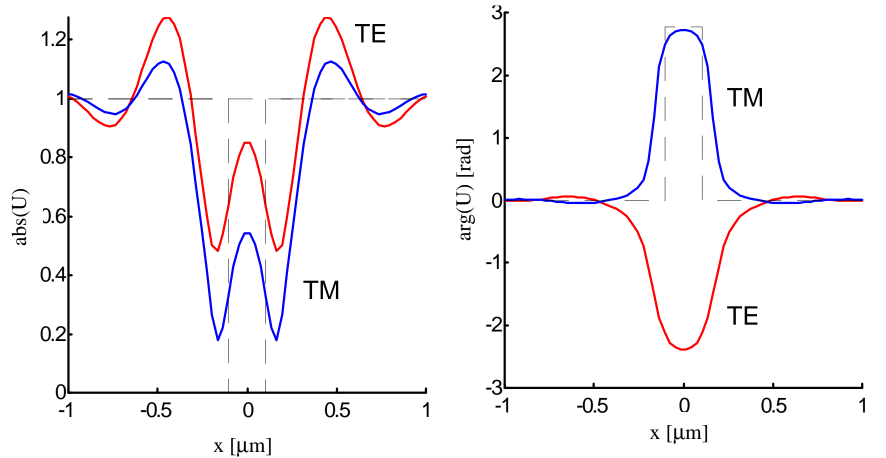

Fig. 9 Computed amplitude (left) and Phase (right) of a Si-bar of 210 nm width and 121nm height on Si for TE and TM polarization

4. PHYSICAL-OPTICS MODELS

In a rather simplified manner we may say that the phase image of a pure topographical structure represents the topography, the amplitude image the amount of scattering beyond the imaging NA and the polarization effect the difference of boundary conditions for both orthogonal polarizations. These are most pronounced for edges and inclined sections.

To use the polarization effects for resolution enhancement or at least a better interpretation of the images, their origin should be understood in terms of simple physical-optics models. Of course it is possible, as was demonstrated in the preceding section, to compute the images rigorously and to include by this means vector aspects into the analysis. But to our opinion this is more useful for systematical investigations and eventually providing a kind of look-up table (polarization effect vs. structure parameter). For the development of sensor concepts using these effects a more „operational understanding“ is necessary. In the following two subsections we discuss rather simple models to explain the observed effects

4.1 Boundary diffraction wave

The concept of the boundary diffraction wave dates back to T. Young. The basic idea is to consider diffraction (U_{diff}) as a deviation from the geometrical optics propagation (U_{g}). This is due to a boundary diffraction wave[13] U_{BDW} originating from the rim of the aperture or in our case from the structure edges.

$$U_{\mathrm{diff}} = U_{\mathrm{g}} + U_{\mathrm{BDW}} \qquad (15)$$

U_{BDW} is discontinuous to compensate for the discontinuity of the geometrical optics field. Polarization dependent boundary diffraction waves from diffraction by perfect conductors are well known.[14] This model was used by Kimura and Wilson[5] to understand the contrast mechanism of confocal microscopy between crossed polarizers („polarization dark-field“).

Because for perpendicular incidence and vertical edge walls the geometrical optics fields are identical for both polarizations, this concept is useful to describe the difference of differently polarized images. Fig. 10 shows the difference of the rigorously computed near-field and the geometrical optics near-field for both linear polarizations and two step heights in silicon. The geometrical optics field was computed according to the thin film matrix theory (TFMT[15]).

In Fig. 10 the magnitude of the real part of the electric near-field is plotted. It represents the field amplitude at a certain moment. It visualizes by this means both amplitude and phase of the field.

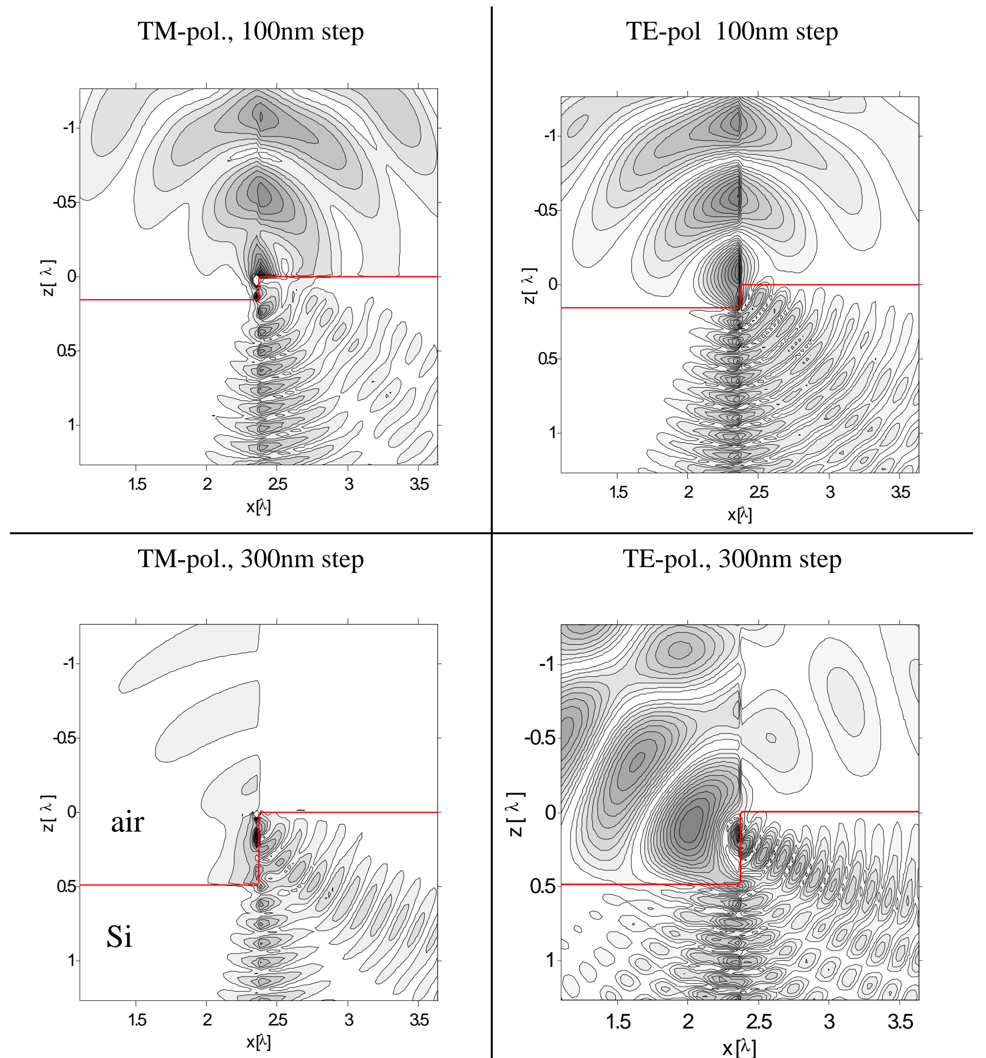

Fig. 10 Nearfield (magnitude of real part of electric field) of the boundary diffraction wave (U_{diff}-U_{g}) at steps of different heights in Si, λ=549nm.. Identical color-maps.

If the concept of the boundary wave is valid, we should observe a cylindrical wave originating from the structure edge. This is approximately true, but the wave is more asymmetrically in TE- than in TM-polarization, in particular for the 300nm step. There the reflected boundary diffraction wave is very weak in TM- but quite strong in TE-polarization. To these effects we attribute the observation that the assumption of a geometrical-optics structure reflection provides better agreement with measured images in TM than in TE polarization.

4.2 Waveguiding

As was demonstrated in section 3.2, sub-wavelength bars and trenches of identical width and height resp. thickness are imaged rather differently. These effects may be understood quantitatively by investigation of the corresponding structure nearfields. A qualitative explanation relies on waveguiding effects. In this section we present preliminary results of an investigation of this topic.

The main idea is to consider the sub-wavelength structures as short waveguides situated on (or in) the substrate. Due to its upper and lower boundaries such a structure forms a resonator that is excited by the incident wave. As is well known the excitation is polarization dependent. In particular for trenches of width w in a perfect conductor there is for excitation in TE-polarization (electric field parallel to the edges) a cut-off (free-space) wavelength of λ=2w because the tangential electric field has to vanish at the walls. For a perpendicular electric field (TM-Polarization) there is no cut-off frequency because the electric field component is oriented normal to the structure edges. Hence, the lowest order mode may penetrate into the groove for TM polarization while it is evanescent and therefore strongly attenuated for TE-polarization. Such a model was already used qualitatively by Marx and Psaltis for explanation of the polarization interferometrical detection of DVD pits.[16]

The same argument applies approximately for a strong dielectricum as is demonstrated in Fig. 11. There, the amplitude of electric nearfield for TM-polarization (left) and TE-polarization (right) is shown for a perpendicularly incident plane wave and a trench of 0.16λ width and 0.4λ depth in Si (λ=500 nm, n=4.18+i*0.3). The different penetration depth is clearly visible. However, for a weaker dielectrica like glass the effect is considerably weaker.

For bars on a substrate the argument may be applied in a modified form. Now the structure is considered as a short film-waveguide consisting of a high-index film in a low-index medium. It is excited by the incident wave. Responsible for the polarization effects are now their different mode-wavelengths. These are easily obtained from standard textbooks[17] for a film of thickness d and refractive index n_f in a medium with refractive index n_0 by solution of

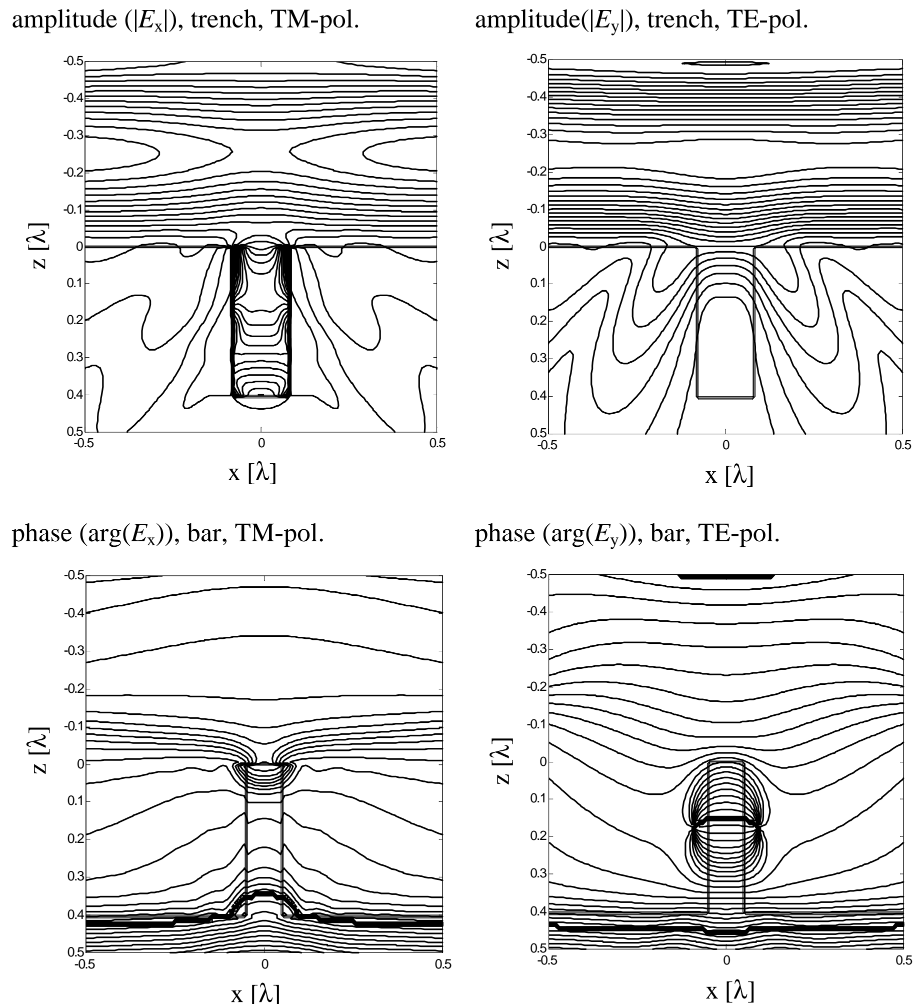

Fig. 11 Field penetration into a trench in Si (top, amplitude isolines), phase of Si-bar on Si (bottom, phase-isolines).

$$\tan(u - m\pi) = \frac{2uv}{q^2u^2 - q^{-2}v^2} \qquad (16)$$

with the mode-number m, $u = \left((n_f k_0^2) - \beta^2\right)^{1/2} d$,

$v = \left(\beta^2 - (n_0 k_0)^2\right)^{1/2} d$, $k_0 = 2\pi\lambda^{-1}$, $q = n_0/n_f$ and the mode-wavelength $\lambda_M = 2\pi/\beta$. The mode-diagram is plotted in Fig. 12. The thin line shows the relative mode-wavelength for TE-polarization and the thick-line for TM-polarization.

For a given mode, the mode-wavelength decreases faster with increasing width for TE polarization, providing a comparatively stronger phase-shift.

Summing up: the waveguiding effects are responsible for the observed opposite behavior of sub-λ bars and trenches in imaging. Bars provide a stronger phase-shift in TE-polarization because of the lower mode-wavelength. Trenches yield a stronger phaseshift for TM-polarization because of the higher penetration depth.

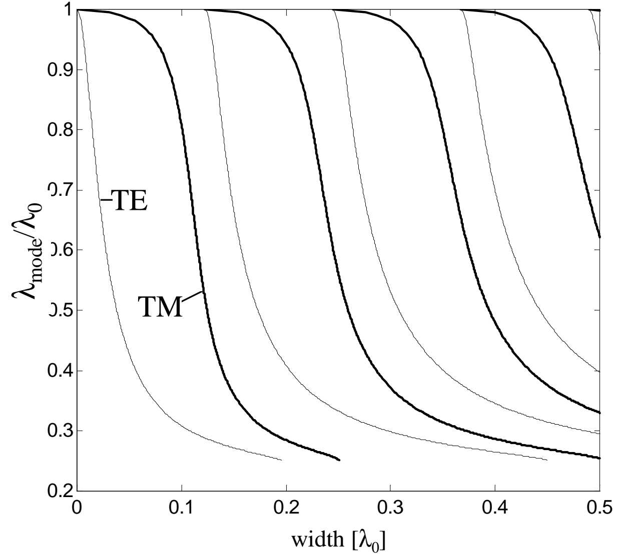

Fig. 12 Mode-diagram for Si film-waveguides at λ=500nm

5. POLARIZATION INTERFEROMETRY

According to the preceding sections, the relative phase-shift between the TE and TM polarized components is an important polarization effect in particular for sub-wavelength structures. It can be measured directly by polarization-interferometry , i.e. instead of superposing the fields reflected by the object and an external reference as in conventional interference-microscopy, we interfere the TE- and the TM-polarized image of the same structure. Phase and contrast are measured using temporal phase shifting. Of course, we loose the height information but, as we will show, we gain an increased edge sensitivity. Furthermore, the method is less sensitive to vibrations because it constitutes basically a common-path interferometer.

The experimental set-up for polarization interferometry is based on a Leica DMR microscope (Fig. 13) with an attached laser-illumination and a detection unit mounted on the photo-tubus. The non-polarizing components form a reflection-type microscope with a two-step magnifying system. The illumination consists of a laser-diode of wavelength λ=635nm (Sanyo DL3038023, 3mW) that is collimated and focused with f/D=4 onto a rotating ground-glass. The laser-diode is driven near its threshold to reduce the temporal coherence. The spatial coherence is adjustable via the diameter of the illuminated spot on the ground glass. The ground glass is imaged into the aperture-stop of the Köhler illumination system of the microscope. Due to experimental constraints it was necessary to insert the polarizer λ/4 plate combination between laser-diode and focus lens. This somewhat unusual configuration worked well, most likely because we applied a small roughness ground-glass with an NA of approximately 0.5. To estimate the depolarization we measured the contrast of polarization-interferograms without and with the ground-glass. The contrast differed by less than 1%.

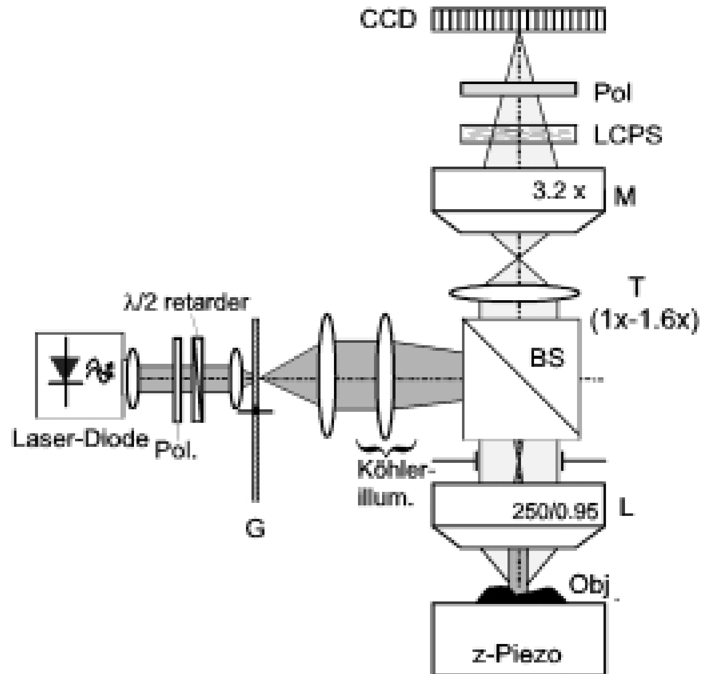

Fig. 13 Set-up for microscopical polarization-interferometry. G=rotating ground.glass, L= microscope lens, T=tube-lens, M additional magnification, BS: non-polarizing beam-splitter, LCPS: liquid crystal phase-shifter, Pol: polarizer

The image of the structure due to a 250/0.95 lens and tube lens (magnification: M_T=1.0, 1.25, 1.6) is projected by a 3.2× magnifying lens *L* (NA=0.15) onto a CCD-Chip (Hitachi KP160). The overall magnification amounts at M_T=1.25 to 1000, i.e. a single 9.2×8.4 μm^2 pixel on the CCD corresponds to a 9.2nm × 8.4nm pixel in the object space. The high magnification is necessary to resolve the observed steep edge images. Additonally it allows a strong noise-reduction (c.f. section 2.1) The focus-position can be adjusted with nm-accuracy by a capacitive-sensor controlled piezo translation-stage (Physik Instrumente).

The electrooptic compensator consists of a liquid crystal phase-shifter (LCPS), i.e. a planar nematic liquid-crystal cell between two transparent ITO electrodes (Jenoptik). The maximum phase-shift is ≈6π at λ=635nm. The TE and TM field-components interfere at the polarizer behind the LCPS. The resulting interferogram on the CCD chip is transferred via a 10bit frame-grabber to the computer. Image acquisition and interferogram evaluation are identical to the above described conventional interference microscopy, as described in section 2.1.

A measurement example is shown in Fig. 14. The illumination-NA is 0.4. In particular the contrast image indicates distortions rather sensitively, compared with the intensity image.

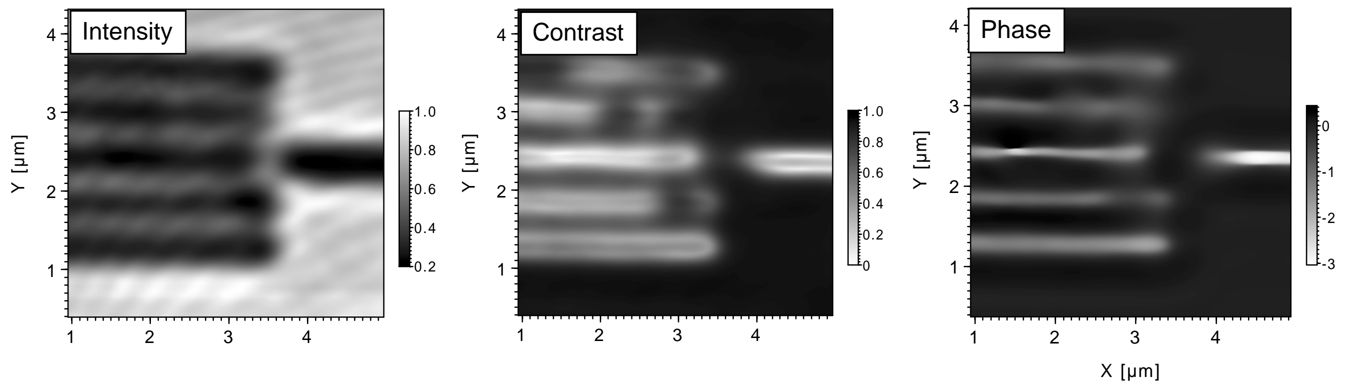

Fig. 14 Intensity (a), contrast(b), and phase-image (c) of 5 trenches of 120nm depth and 600nm pitch in Si.

6. CONCLUSIONS

Interference microscopy at different orthogonal polarizations with temporal phase shifting can be used for a systematical investigation of polarization effects observed at linear microstructures. We have shown that the evaluation provides the diagonal elements of the Jones-matrix. In the absence of non-diagonal elements, subsequent defocus and image-contrast generation is possible according to a „synthetical microscopy“. The agreement with rigorous numerical simulations according to the RCWA is satisfactorily. Using near-field computations, we have shown that for steps and narrow trenches in Si, TM-polarization provides a considerably better agreement with geometrical optics than TE-polarization. Polarization interferometry measures directly the phase-shift between the TE- and TM-polarized fields. By this means it provides a sensitive method for linewidth-measurements of topographical microstructures.

REFERENCES

1. D.Nyyssonen, "Linewidth measurement with an optical microscope: the effect of operating conditions on the image profile", *Appl. Opt*. **16**, pp. 2223-2230 (1977).
2. K.-P. Schröder, W. Mirandé, H. Geuther, C. Herrmann, "In quest of nm accuracy: supporting optical metrology by rigorous diffraction theory and AFM topography", *Opt. Commun.* **115,** pp. 568-576 (1995).
3. P. Lalanne, P. Pichon, E. Chavel, E. Cambril, H. Launois, "Interferometrical characterization of subwavelength lamellar gratings", *Appl. Opt.* **38**, pp. 4980-4984 (1999).
4. R. Barakat, "Optical linewidth measurements using a polarized microscope with crossed polarizers", *Appl. Opt*. **29**, pp. 5038-5039 (1990).
5. S. Kimura, , T. Wilson, "Confocal scanning dark-field polarization microscopy", *Appl. Opt*. **33**, pp. 1274-1278 (1994).

6. M. Totzeck, H.J. Tiziani, "Phase-shifting polarization-interferometry for microstructure linewidth measurements", *Opt. Lett.* **24**, 294-296 (1999).
7. J. Schmit, K. Creath, "Window function influence on phase error in phase-shifting algorithms", *Appl. Opt.* **35**, pp. 5642-5649 (1996).
8. K. Creath, "Calibration of numerical aperture effects in interferometric microscopy objectives", *Appl. Opt*. **28**, pp. 3333-3338 (1989).
9. E.D.Palik, *Handbook of Optical Constants of Solids*, Academic Press 1985, 547ff.
10. M.G. Moharam, E.B. Grann, D.A. Pommet, T.K. Gaylord, "Formulation for stable and efficient implementation of the rigorous coupled-wave analysis of binary gratings", *J. Opt. Soc. Am. A* **12,** pp. 1068-1076 (1995)
11. H. H. Hopkins, "Image Formation with partially coherent light", *Photogr. Sci. and Eng*. **21,** pp.114-123 (1977).
12. M. Totzeck, H.J. Tiziani, "Phase-singularities in 2D diffraction fields and interference-microscopy", *Opt. Commun.* **138**, pp. 365-382 (1997).
13. M. Born, E. Wolf, *Principles of Optics*, Pergamon Press 1980, 6th Ed. pp. 449f.
14. G. A. Deschamps, J. Boersma, S.-W. Lee, "Three-dimensional half-plane diffraction: Exact solution and testing of uniform theories", *IEEE Transact. Ant. & Prop*. **AP-32**, pp. 264-271 (1984).
15. J. Chilwell, I. Hodgkinson, "Thin-films field-transfer matrix theory of planar multilayer waveguides and reflection from prism-loaded waveguides", *J. Opt. Soc. Am. A* **1**, pp. 742-753 (1984)
16. D.S. Marx, D. Psaltis, "Polarization quadrature measurement of subwavelength diffracting structures", *Appl. Opt.* **36**, pp. 6434-6440 (1997).
17. Textbooks on waveguide theory, for instance: H. G. Unger, *Optische Nachrichtentechnik I*, Huethig 1993 (in German).
18. The term „image“ is used in a rather general sense here. It is a collection of spatially dependent data f(x,y) derived from a microscopical measurement. Without prefix it denotes the complex, electric field component in the image plane. Particular field quantities or combinations of them are characterized by the appropriate prefix: Phase-image, itensity-image, contrast-image etc..
19. T.R. Corle, G.S. Kino, *Confocal Scanning Optical Microscopy* (Academic, San Diego, 1996) pp. 286f.